nature materials

LETTERS

PUBLISHED ONLINE: 1 JULY 2012 | DOI: 10.1038/NMAT3370

The nature of strength enhancement and weakening by pentagon–heptagon defects in graphene

Yujie Wei[1]*, Jiangtao Wu[1], Hanqing Yin[1], Xinghua Shi[1], Ronggui Yang[2]* and Mildred Dresselhaus[3]

The two-dimensional crystalline structures in graphene challenge the applicability of existing theories that have been used for characterizing its three-dimensional counterparts. It is crucial to establish reliable structure–property relationships in the important two-dimensional crystals to fully use their remarkable properties. With the success in synthesizing large-area polycrystalline graphene[1–5], understanding how grain boundaries (GBs) in graphene[2–4] alter its physical properties[5–13] is of both scientific and technological importance. A recent work showed that more GB defects could counter intuitively give rise to higher strength in tilt GBs (ref. 10). We show here that GB strength can either increase or decrease with the tilt, and the behaviour can be explained well by continuum mechanics. It is not just the density of defects that affects the mechanical properties, but the detailed arrangements of defects are also important. The strengths of tilt GBs increase as the square of the tilt angles if pentagon–heptagon defects are evenly spaced, and the trend breaks down in other cases. We find that mechanical failure always starts from the bond shared by hexagon–heptagon rings. Our present work provides fundamental guidance towards understanding how defects interact in two-dimensional crystals, which is important for using high-strength and stretchable graphene[14] for biological and electronic applications.

Among the remarkable physical properties[15–20] observed in graphene, the high strength reported in pristine graphene[19] is stimulating great interest in applying high strength and stretchable graphene for various applications such as in biological membranes and electronic devices[14]. For example, monolayer graphene can have a loading capacity comparable to a 50-nm-thick film (for example, copper or silicon) with a strength of about 200 MPa. However, the presence of GBs in large-area polycrystalline graphene raises a fundamental question as to whether polycrystalline graphene for engineering practice can be as strong as pristine graphene. Although there is a good understanding on how typical defects such as dislocations and GBs influence the strength of three-dimensional polycrystals, how GB defects such as pentagon–heptagon rings in two-dimensional graphene influence its mechanical properties remains unknown. In this work, we address how and why pentagon–heptagon defects in a tilt GB may enhance or weaken the strength of graphene through both molecular dynamics (MD) simulations and continuum mechanics analysis.

To gain some insight into the influence of GB defects on the mechanical strength of graphene, we perform MD simulations for the dependence of GB strengths on grain misorientation for graphene with both armchair and zigzag tilt GBs. Simulation details are given in the Methods and Supplementary Information. At the atomic level, GBs in graphene are usually formed by typical defects of pentagon–heptagon rings[5–13]. We construct a series of both low-angle and high-angle tilt GBs (Supplementary Figs S1 and S2) based on the disclination dipole model[21]. For tilt GBs composed of evenly spaced pentagon–heptagon rings (disclination dipoles) with disclination strength ω and characteristic height h_d, we could calculate the GB tilt angle θ as[21]

$$\theta = \omega h_d / L \quad (1)$$

where L is the spacing between two dipoles.

The stress–strain curves and the corresponding GB normal strengths for graphene with armchair and zigzag tilt GBs at different tilt angles θ are shown in Fig. 1a,b, respectively. For zigzag tilt GBs, GB strength increases with θ. In armchair tilt GBs, however, the trend is not monotonic. Pentagon–heptagon rings are not uniformly spaced (Supplementary Fig. S1d,e) in armchair tilt GBs to form tilt angles at $\theta = 16.4$ and 17.9, which results in the breakdown in the belief that the strength in graphene increases monotonically with defect density[10]. Also, GB normal strengths are less sensitive to θ for $5° < \theta < 17.9°$ in armchair tilt GBs than in zigzag tilt GBs. In Fig. 1c, we show the GB energy γ as a function of tilt angle. In general, increasing tilt angles (hence more GB defects) lead to a higher GB energy. Meanwhile, local structure relaxation and defect interaction can effectively lower the GB energy. The competition between these two mechanisms results in a maximum in GB energy with tilt angle, as shown in Fig. 1c. We note that the cancellation of bond pre-strain and strain energy by means of defect interaction has also been discussed recently[22,23].

The non-monotonic change of the strength with tilt angle in armchair tilt GBs (Fig. 1b) is intriguing. In contrast to other cases, GBs with $\theta = 16.4°$ (Supplementary Fig. S1d) and 17.9° (Supplementary Fig. S1e) do not have the same periodic characteristics of pentagon–heptagon defects in the GBs. From a geometrical perspective, a pentagon–heptagon pair resembles a disclination dipole[21,24–26], which consists of two disclinations of opposite signs. These armchair tilt GBs under present consideration are either composed of an array of uniformly distributed disclination dipoles (Fig. 2a) or an array of disclination dipole clusters (Fig. 2c,e). MD simulations are then used to calculate the stress contours, as shown, respectively, in Fig. 2b,d,f, for the corresponding GBs shown in

[1]LNM, Institute of Mechanics, Chinese Academy of Sciences, Beijing 100190, China, [2]Department of Mechanical Engineering, University of Colorado, Boulder, Colorado 80309, USA, [3]Department of Physics and Electrical Engineering, Massachusetts Institute of Technology, Cambridge, Massachusetts 02139, USA. *e-mail: Yujie_Wei@lnm.imech.ac.cn; ronggui.yang@colorado.edu.

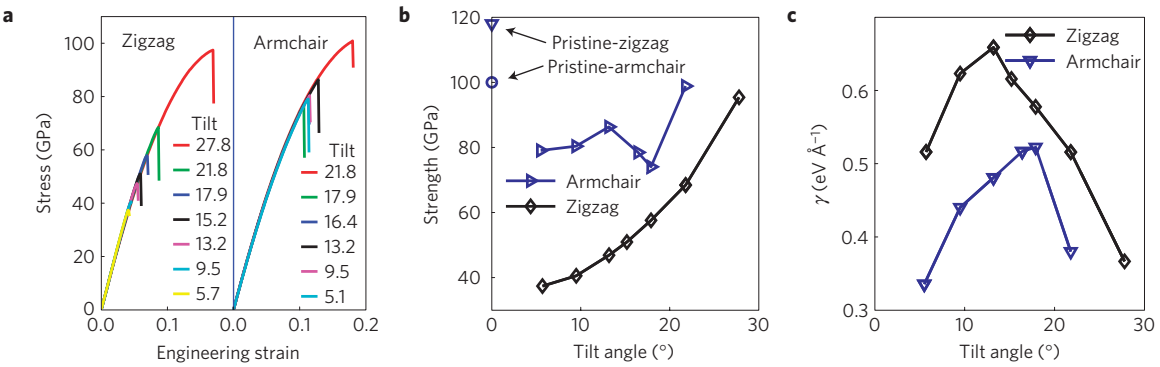

Figure 1 | Stress–strain behaviour and GB energy in both armchair and zigzag tilt GBs. a, Stress–strain behaviour of zigzag tilt GBs (left) and armchair tilt GBs (right) at different tilt angles. **b**, GB normal strength as a function of tilt angle. The two isolated points are the strengths of pristine graphene stretching in zigzag ('open down triangle') and armchair ('open circle') directions, respectively. **c**, GB energy as a function of tilt angle.

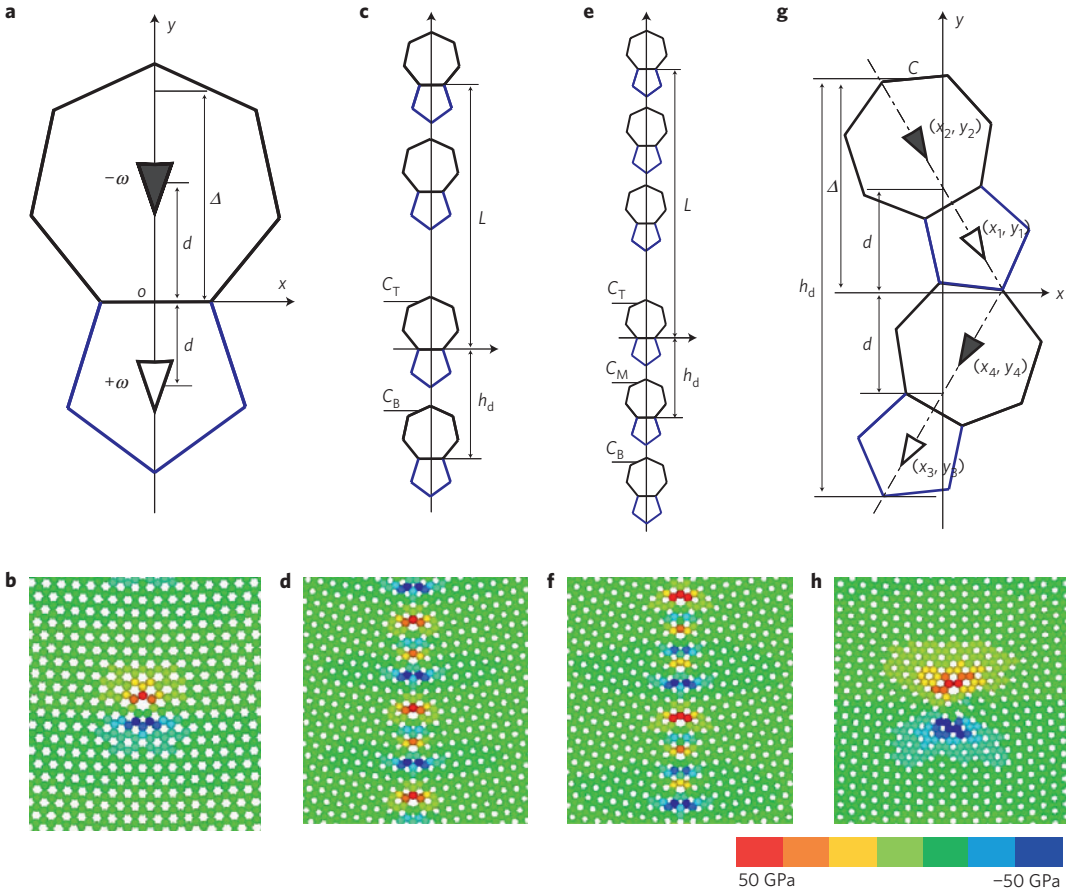

Figure 2 | Typical defects and their stress fields in tilt GBs in graphene from MD simulations. a, A disclination dipole formed by a pentagon–heptagon defect. The idea in ref. 27 is used to denote the feature of each disclination, with open down and filled down triangles representing, respectively, the removal and the insertion of a material wedge. Removing a wedge followed by inserting a counterpart forms a disclination dipole if their tips are separated by 2*d*, which resembles an edge dislocation with a Burgers vector $b = 2\omega d$ (refs 21,27). Regular armchair tilt GBs are formed by evenly spaced disclination dipoles. **c**,**e**, Armchair tilt GBs with tilt angles $\theta = 16.4°$ and $\theta = 17.9°$ formed by evenly displaced disclination clusters, with each cluster containing two and three disclination dipoles, respectively. With *a* being the C–C bond length, $L = 2h_d + 3a$ for the GB in **c** and $L = 3h_d + 3a$ for **e**. **g**, Disclination clusters in zigzag tilt GBs. **b**,**d**,**f**,**h**, Normal stress contours induced by defects from **a**,**c**,**e** and **g**, respectively.

Fig. 2a,c,e. For the stress induced by disclination clusters (Fig. 2c,e), we notice that the top-most dipole in a cluster has the highest normal stress σ_{xx} (Fig. 2d,f). We will explain the mechanism behind this in the following text. In comparison, zigzag tilt GBs are formed by evenly spaced disclination clusters, as shown in Fig. 2g, where the stress induced by the disclination clusters (Fig. 2h) is much greater than that by the disclination dipole in Fig. 2b. If we make an analogy between the disclination dipoles and dislocations, disclination clusters in Fig. 2g have a larger equivalent Burgers vector than that of the disclination dipoles in Fig. 2a.

Being rotational defects, disclinations show great advantages in capturing the mechanical behaviour in GBs (refs 24–26), in contrast to dislocation mechanisms. Similar to dislocations, disclinations induce long-range stress fields and interact with other defects[21,24–27].

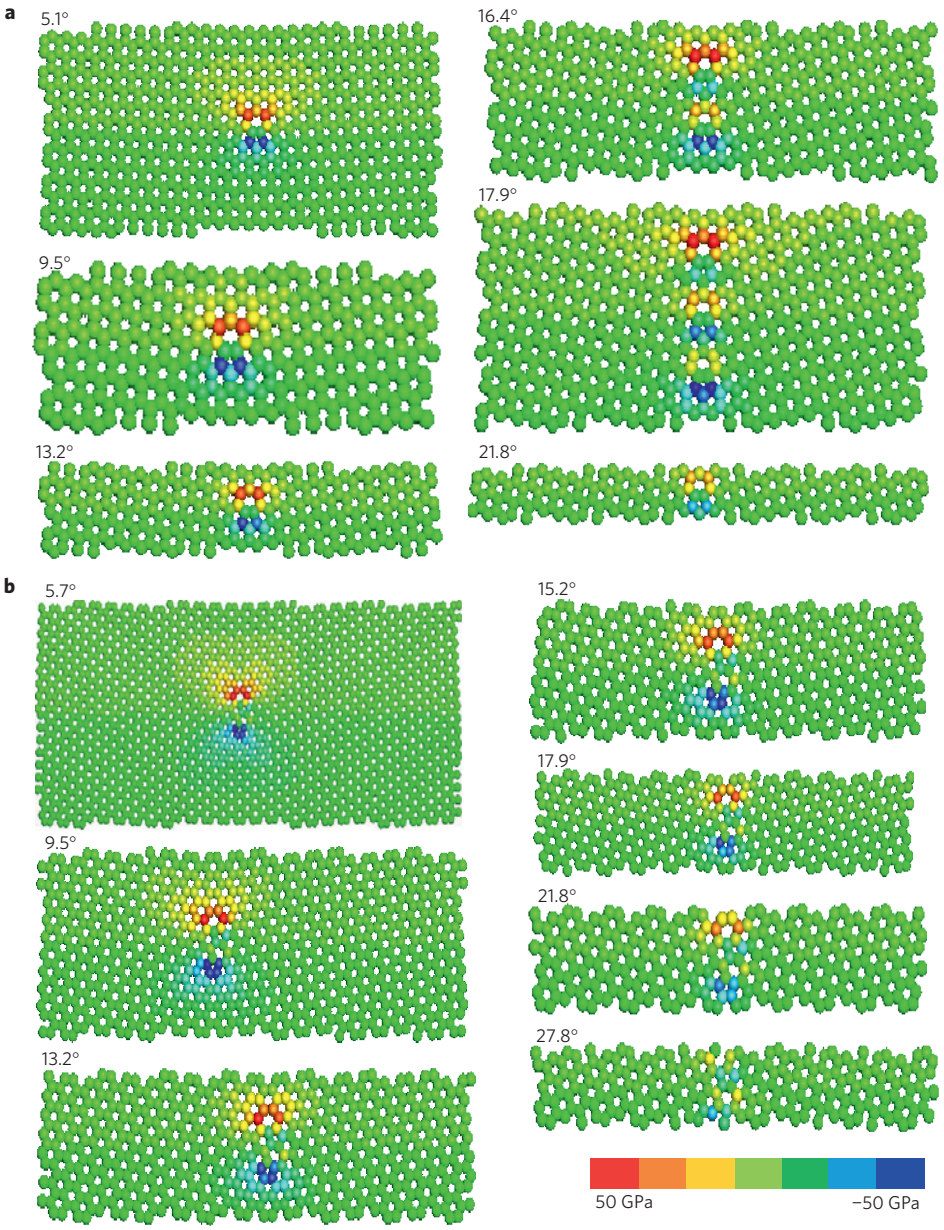

Figure 3 | Normal stress contour (from the disclination dipole model) for tilt GBs at different tilt angles. The tilt angles θ are labelled in each figure. One periodicity is used as noted for each GB structure. The contour bar is given in the middle. **a**, Armchair tilt GBs. Maximum tensile stress in the bond shared by hexagon–heptagon pairs decreases, increases, and then decreases again as the tilt angle increases. **b**, Zigzag tilt GBs. Maximum tensile stress monotonically decreases as the tilt angle increases.

Ref. 21 supplied the stress field induced by a single dipole (Supplementary Equation S1) with the positive and negative wedge disclinations residing at $(0,-d)$ and $(0,d)$, respectively. Similar to references[21,24–27], we can define a pentagon (heptagon) ring as a positive (negative) disclination in GBs (Fig. 2a). We note that defect-induced warping in suspended graphene[22,23] challenges the applicability of the disclination dipole model that was originally developed for plane deformation. However, our analysis (see Supplementary Information S5) shows that an initial elastic stretch can effectively suppress warping. It has been validated by our MD simulations that the stress field induced by a pair of pentagon–heptagon rings can be described well by the disclination dipole model (see Supplementary Information S4). This ensures the effectiveness of the disclination dipole model in predicting the strength of graphene with pentagon–heptagon defects. The stress component perpendicular to a GB, σ_{xx}, is of interest as it directly influences the GB normal strength. With the relaxed GB structures coming from our MD simulations (Supplementary Figs S1 and S2), we can now conveniently apply the disclination dipole theory (see Supplementary Equation S1 for armchair tilt GBs and Supplementary Equation S3 for zigzag tilt GBs) to obtain σ_{xx} in each bond. For the Cartesian coordinate shown in Fig. 2a, we are interested in the summation of the normal stress produced by an infinite array of pentagon–heptagon defects. Figure 3a shows the computed normal stress contours for armchair tilt GBs for different tilt angles. The maximum tensile stress appears in the bond shared by hexagon–heptagon rings, which decreases, increases, and then decreases again as the tilt angle increases. The deviation from the monotonic increase occurs when the disclination dipoles are not evenly spaced (see Fig. 2c for $\theta = 16.4°$ and Fig. 2e for $\theta = 17.9°$). Figure 3b shows the stress contours induced by pentagon–heptagon defects for zigzag tilt GBs, where the peak tensile stress appears in the bond shared by hexagon–heptagon

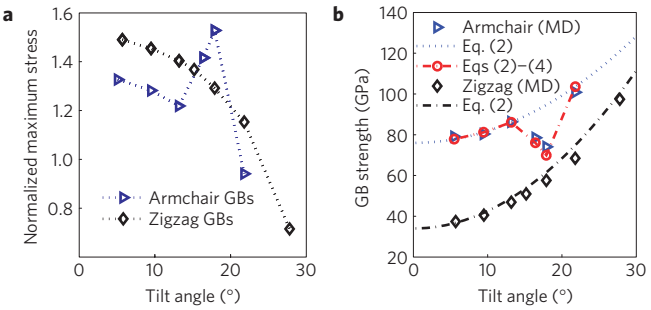

Figure 4 | Dependence of initial maximum GB tensile stress and GB strength on tilt angles. a, Initial maximum tensile stresses (at the bond shared by hexagon–heptagon rings and normalized by $E\omega/4\pi$) versus tilt angles in armchair and zigzag tilt GBs. **b**, The comparison of the theoretical prediction and results of MD simulations for GB normal strength as a function of tilt angle. Dotted and dashed curves given by equation (2) are, respectively, for armchair and zigzag tilt GBs with evenly spaced disclination dipoles. They match well with MD simulations. The strengths for armchair tilt GBs with $\theta = 16.4°$ and $\theta = 17.9°$, where disclination dipoles are not uniformly distributed, can be described well by equations (3) and (4) (red circles guided by the dashed line), respectively.

pairs and the stress decreases monotonically as θ increases. These theoretical results are consistent with MD simulations in Fig. 1 and can be used to explain why failure always is initiated at hexagon–heptagon pairs in MD simulations (Supplementary Fig. S4).

The maximum tensile stress values as a function of tilt angle for both armchair and zigzag tilt GBs are shown in Fig. 4a. The change in the maximum tensile stress by continuum theory, which regards pentagon–heptagon rings as disclination dipoles, is exactly opposite to the variation in GB strength in Fig. 1b. Figure 4a clearly explains that stress relaxation induced by defect interactions controls the strength–tilt angle relationship, as seen in Fig. 1b, because an increase in tensile stress of a GB would result in a reduction in GB normal strength.

Now we aim to derive a more straightforward formula for the strength–tilt angle correlation in tilt GBs. The same array of evenly spaced pentagon–heptagon defects in armchair tilt GBs (with periodicity L) is considered, and the y axis of the coordinate passes through the core of all disclination dipoles, as shown in Fig. 2a. Normal stress s_{xx} at $(0, \Delta)$—the bond shared by the hexagon–heptagon pairs—is derived to have an asymptotic expression of: $s_{xx}/\sigma_0 = -2\pi^2 \Delta d/3L^2$ (see Supplementary Information S6), where $\sigma_0 = E\omega/4\pi$, E is the Young modulus, ω is the rotational strength of the disclination, and Δ is the distance from the origin to the shared bond. Different to σ_{xx}, s_{xx} does not include the stress from the disclination dipole under consideration. We further note that the tilt angle θ is related to L as $\theta = \omega h_d/L$ in equation (1). We can hence write s_{xx}/σ_0 in terms of θ as

$$\frac{s_{xx}}{\sigma_0} = -\frac{2\pi^2 \Delta d}{3h_d^2}\frac{\theta^2}{\omega^2} \qquad (2)$$

Several features are captured in equation (2). First, the compressive stress at positive Δ (above the origin, on the side of the negative disclination) increases as θ increases. As the self-stress (at $y = \Delta$) of the disclination dipole is tensile, equation (2) indicates that the remaining disclination dipoles will reduce the tensile stress at $y = \Delta$ by a net compression, which effectively increases the strength of the GB when failure is initiated at $y = \Delta$. Second, disclination dipoles with a larger separation result in less compressive stress at $y = \Delta$, and lead to a lower GB strength. And third, the superimposed compressive stress is proportional to θ^2 (that is, inversely proportional to L^2).

For evenly spaced disclination clusters, for example, armchair tilt GBs with $\theta = 16.4°$ (Fig. 2c) and $\theta = 17.9°$ (Fig. 2e), stress at

Table 1 | The geometrical and material parameters used for equations (2) to (4) to obtain the theoretical curves shown in Fig. 4b for both armchair and zigzag tilt GBs.

Name	ω	Δ	h_d	d	σ_{y0}
Units	(°)	(a)	(a)	(a)	(GPa)
Armchair	21.8	1.5	4.7	0.8	76
Zigzag	27.8	3.2	6.3	1.5	33

Here, ω is the rotational strength of a disclination, Δ is the distance from a disclination dipole centre to the critical hexagon–heptagon bond, h_d is the characteristic height of a disclination dipole in armchair tilt GBs and the height of the unit disclination cluster shown in Fig. 2g in zigzag tilt GBs, d is the half-distance between disclination centres, σ_{y0} is the strength of the hexagon–heptagon bond in a disclination dipole without the influence of other dipoles and a is the bond length of carbon–carbon atoms. Based on experiments[19], we take Young's modulus as $E = 1{,}050$ GPa for pristine graphene.

$y = \Delta$ by the remaining disclination dipoles is obtained by using equation (2) and the stress-field of a disclination dipole[21]. For the armchair tilt GB with $\theta = 16.4°$, the extra amounts of stress in the top (C_T in Fig. 2c) and bottom dipoles (C_B) are given, respectively, by equations (3a) and (3b).

$$\left(\frac{s_{xx}}{\sigma_0}\right)_T = -\frac{2\pi^2 \Delta d}{3L^2} - \frac{2\pi^2 (h_d + \Delta) d}{3L^2} + \ln\left(\frac{h_d + \Delta + d}{h_d + \Delta - d}\right) \qquad (3a)$$

$$\left(\frac{s_{xx}}{\sigma_0}\right)_B = -\frac{2\pi^2 \Delta d}{3L^2} + \frac{2\pi^2 (h_d - \Delta) d}{3L^2} - \ln\left(\frac{h_d - \Delta + d}{h_d - \Delta - d}\right) \qquad (3b)$$

Similarly, for the armchair tilt GB with $\theta = 17.9°$, the values for the extra tensile stress to the hexagon–heptagon bonds in dipoles at the top (C_T in Fig. 2e), middle (C_M), and bottom (C_B) of a cluster are given respectively by equations (4a)–(4c):

$$\left(\frac{s_{xx}}{\sigma_0}\right)_T = -\frac{2\pi^2 (h_d + \Delta) d}{L^2} + \ln\left[\frac{h_d + \Delta + d}{h_d + \Delta - d}\,\frac{2h_d + \Delta + d}{2h_d + \Delta - d}\right] \qquad (4a)$$

$$\left(\frac{s_{xx}}{\sigma_0}\right)_M = -\frac{2\pi^2 \Delta d}{L^2} + \ln\left[\frac{h_d^2 - (\Delta + d)^2}{h_d^2 - (\Delta - d)^2}\right] \qquad (4b)$$

$$\left(\frac{s_{xx}}{\sigma_0}\right)_B = \frac{2\pi^2 (h_d - \Delta) d}{L^2} - \ln\left[\frac{h_d - \Delta + d}{h_d - \Delta - d}\,\frac{2h_d - \Delta + d}{2h_d - \Delta - d}\right] \qquad (4c)$$

These equations tell us that the hexagon–heptagon pair in the topmost dipole of a cluster is usually subjected to the highest tension, which is consistent with our MD simulations. A detailed derivation of equations (3) and (4) is given in Supplementary Information S6.

With equations (2)–(4), we are ready to explain all the details of the strength–tilt angle relationship in Fig. 1b. The GB strength is determined by the strength of a disclination dipole without the influence of the other defects in the sample, minus the stress applied by all other disclination dipoles, that is, $\sigma_y = \sigma_{y0} - s_{xx}$. Here σ_{y0} is about 76 GPa for armchair tilt GBs (Fig. 2a,c,e) and 33 GPa for zigzag tilt GBs (Fig. 2g). The difference in strength σ_{y0} is due to the differences in the equivalent Burgers vectors (Fig. 2b,h) and in the orientations of the bond shared by the hexagon–heptagon rings (Fig. 2a,g). In Fig. 4b, we show both the theoretical predictions and the results from MD simulations (triangles for armchair tilt GBs and diamonds for zigzag tilt GBs). The theoretical prediction using equation (2), with the material parameters listed in Table 1, shown using the dotted and dashed curves for armchair and zigzag tilt GBs, respectively, matches very well with MD simulations for tilt GBs with evenly spaced disclination dipoles. However, the strength for armchair tilt GBs with $\theta = 16.4°$ and $\theta = 17.9°$ cannot be captured

by equation (2), but are described well by equations (3) and (4) (red circles guided by the dashed line), respectively.

In conclusion, we find that GB defects can either strengthen or weaken graphene, which relies on the detailed arrangement of the defects, not just the density of defects. Given the polar nature of the stress field induced by a disclination dipole (Supplementary Fig. S7), the distribution of other disclination diploes in a GB may produce a stress field to either increase or decrease[23] the self-stress of the disclination dipole under consideration. Through both MD simulations and continuum mechanics analysis, we show that the strengths of tilt GBs increase as the square of their tilt angles if pentagon–heptagon defects are evenly spaced, and that the trend breaks down if pentagon–heptagon defects are not evenly distributed. Mechanical failure always starts from the bond shared by the hexagon–heptagon rings in tilted GBs, not the bond that is shared by pentagon–heptagon rings. Given that pentagon–heptagon rings are one of the most common defects in carbon nanotubes, fullerenes and graphene[28], the theoretical analysis given here will advance the understanding of defect interactions in carbon nanostructures, and possibly other two-dimensional materials.

Methods

The Adaptive Intermolecular Reactive Empirical Bond Order (AIREBO) Potential[29] for Carbon is used for MD simulations. Following ref. 10, we have also used a switch function parameter $r_{CC} = 1.92$ Å (Table 1 in ref. 29), beyond which a C–C bond breaks. The choice of $r_{CC} = 1.92$ Å in the AIREBO potential[29] is further validated by comparing the density functional theory calculations and MD simulations for the stress–strain curves in pristine graphene in either the armchair or zigzag direction (see Supplementary Information S2 for details).

The Large-scale Atomic/Molecular Massively Parallel Simulator (LAMMPS, ref. 30) is used for our simulations. All simulations are performed at constant atom number (N), volume (V) and energy (E) (NVE) ensemble in LAMMPS (ref. 30), and a simulated system has an initial temperature of 0 K. A constant time step of 1 fs is used. The periodic boundary condition is applied along its horizontal and vertical directions, and no constraint is applied to its thickness direction for the simulation box. Supplementary Fig. S3 shows that the periodic boundary condition in the x-axis and y-axis can be used when anti-symmetrical GBs are generated, and there is no constraint to the z-axis. All samples are about 100 nm in length and 30 nm in width. Before mechanical loading, each sample is completely relaxed to reach an energy minimum with almost zero pressure. Uniaxial tension is then applied along the horizontal direction (perpendicular to the GBs) of the simulated box by uniformly stretching the sample in the horizontal direction, but we allow the box to shrink in the vertical direction (LAMMPS; ref. 30 command: fix/deform). Virial stresses for each atom are calculated. All samples are strained at a strain rate of 10^9 s^{-1}.

Received 25 April 2012; accepted 25 May 2012; published online 1 July 2012

References

1. Li, X. *et al.* Large-area synthesis of high-quality and uniform graphene films on copper foils. *Science* **324,** 1312–1314 (2009).
2. Kim, K. S. *et al.* Large-scale pattern growth of graphene films for stretchable transparent electrodes. *Nature* **457,** 706–710 (2009).
3. Reina, A. *et al.* Large area, few-layer graphene films on arbitrary substrates by chemical vapor deposition. *Nano Lett.* **9,** 30–35 (2009).
4. Park, S. & Ruoff, R. S. Chemical methods for the production of graphenes. *Nature Nanotech.* **4,** 217–224 (2009).
5. Zhao, L. *et al.* Influence of copper crystal surface on the CVD growth of large area monolayer graphene. *Solid State Commun.* **151,** 509–513 (2011).
6. Yu, Q. K. *et al.* Control and characterization of individual grains and grain boundaries in graphene grown by chemical vapour deposition. *Nature Mater.* **10,** 443–449 (2011).
7. Yazyev, O. V. & Louie, S. G. Electronic transport in polycrystalline graphene. *Nature Mater.* **9,** 806–809 (2010).
8. Yazyev, O. V. & Louie, S. G. Topological defects in graphene: Dislocations and grain boundaries. *Phys. Rev. B* **81,** 195420 (2010).
9. Huang, P. Y. *et al.* Grains and grain boundaries in single-layer graphene atomic patchwork quilts. *Nature* **469,** 389–392 (2011).
10. Grantab, R., Shenoy, V. B. & Ruoff, R. S. Anomalous strength characteristics of tilt grain boundaries in graphene. *Science* **330,** 946–948 (2010).
11. Malola, S., Häkkinen, H. & Koskinen, P. Structural, chemical, and dynamical trends in graphene grain boundaries. *Phys. Rev. B* **81,** 165447 (2010).
12. Cockayne, E. *et al.* Grain boundary loops in graphene. *Phys. Rev. B* **83,** 195425 (2011).
13. Kim, P. Graphene: Across the border. *Nature Mater.* **9,** 792–793 (2010).
14. Rogers, J. A., Lagally, M. G. & Nuzzo, R. G. Synthesis, assembly and applications of semiconductor nanomembranes. *Nature* **477,** 45–53 (2011).
15. Novoselov, K. S. *et al.* Electric field effect in atomically thin carbon films. *Science* **306,** 666–669 (2004).
16. Geim, A. K. & Novoselov, K. S. The rise of graphene. *Nature Mater.* **6,** 183–191 (2007).
17. Geim, A. K. Graphene: Status and prospects. *Science* **324,** 1530–1534 (2009).
18. Lin, Y. M. *et al.* 100-GHz transistors from wafer-scale epitaxial graphene. *Science* **327,** 662 (2010).
19. Lee, C., Wei, X., Kysar, J. W. & Hone, J. Measurement of the elastic properties and intrinsic strength of monolayer graphene. *Science* **321,** 385–388 (2008).
20. Koenig, S. P., Boddeti, N. G., Dunn, M. L. & Bunch, J. S. Ultrastrong adhesion of graphene membranes. *Nature Nanotech.* **6,** 543–546 (2011).
21. Li, J. C. M. Disclination model of high angle grain boundaries. *Surf. Sci.* **31,** 12–26 (1972).
22. Liu, Y. & Yakobson, B. I. Cones, pringles, and grain boundary landscapes in graphene topology. *Nano Lett.* **10,** 2178–2183 (2010).
23. Yakobson, B. I. & Ding, F. Observational geology of graphene, at the nanoscale. *ACS Nano* **5,** 1569–1574 (2011).
24. Romanov, A. E. & Kolesnikova, A. L. Application of disclination concept to solid structures. *Prog. Mater. Sci.* **54,** 740–769 (2009).
25. Kleman, M. & Friedel, J. Disclinations, dislocations, and continuous defects: A reappraisal. *Rev. Mod. Phys.* **80,** 61–115 (2008).
26. Shih, K. K. & Li, J. C. M. Energy of grain boundaries between cusp misorientations. *Surf. Sci.* **50,** 109–124 (1975).
27. Eshelby, J. D. A simple derivation of the elastic field of an edge dislocation. *Br. J. Appl. Phys.* **17,** 1131–1135 (1966).
28. Jia, X., Campos-Delgado, J., Terrones, M., Meunier, V. & Dresselhaus, M. S. Graphene edges: A review of their fabrication and characterization. *Nanoscale* **3,** 86–95 (2011).
29. Stuart, S. J., Tutei, A. B. & Harrison, J. A. A reactive potential for hydrocarbons with intermolecular interactions. *J. Chem. Phys.* **112,** 6472–6486 (2000).
30. Plimpton, S. J. Fast parallel algorithms for short-range molecular dynamics. *J. Comput. Phys.* **117,** 1–19 (1995).

Acknowledgements

The authors acknowledge support from Chinese Academy of Sciences (CAS) and Natural Science Foundation of China (NSFC)#11021262 (Y.W.), NSFC#11023001 (X.S.), Air Force of Scientific Research#FA9550-11-1-0109 (R.Y.) and US Department of Energy#DE-SC0001299/DE-FG02-09ER46577 (M.D.). The simulations are conducted at the Supercomputing Center of CAS.

Author contributions

Y.W., R.Y. and M.D. conceived the project. Y.W. developed the theory. Y.W., J.W., H.Y. and X.S. performed the calculations. Y.W., R.Y. and M.D. analysed the characteristics of defect interactions in graphene and wrote the paper. All authors were involved in data analysis and revision of the paper.

Additional information

The authors declare no competing financial interests. Supplementary information accompanies this paper on www.nature.com/naturematerials. Reprints and permissions information is available online at www.nature.com/reprints. Correspondence and requests for materials should be addressed to Y.W. or R.Y.